PALEOCEANOGRAPHY, VOL. 3, NO. 1, PAGES 113-136, FEBRUARY 1988

PACIFIC PELAGIC PHOSPHORUS ACCUMULATION DURING THE LAST 10 M.Y.

Judith B. Moody

Battelle Memorial Institute
Columbus, Ohio

Louis R. Chaboudy, Jr.[1] and
Thomas R. Worsley

Department of Geological Sciences
Ohio University, Athens

Abstract. As a limiting nutrient to marine life, phosphorus (P) is an effective tracer of today's marine productivity. The distribution of P in marine sediments likewise tracks the history of marine productivity because of its relative insolubility in seawater. $CaCO_3$, biogenic opal, terrigenous sediment, and total P have been measured in cores from nine Pacific sites (Deep Sea Drilling Project (DSDP) 65, 66, 310, 77, 62, 572, 463, 586, and GPC-3) and one subantarctic (DSDP 266) site. These sites were specifically chosen to provide information on biota burial flux changes with time for sedimentary sinks that represent key oceanographic variables, i.e., rate of upwelling, water depth, and carbonate dissolution gradient. The accumulation rates of these components for the last 10 Ma were then calculated from determined core age versus depth plots, core bulk density, and porosity data. The accumulation of P weakly correlates with that of $CaCO_3$, moderately with that of total sediment, and very strongly with carbonate-free accumulation. Two prominent peaks for all components occur at 2-3 Ma and 5-6 Ma, and record the chemical loading of dissolved $CaCO_3$, SiO_2, and P from glacially emergent continental shelves. These results indicate that continental shelf phosphorites form during interglacially high sea levels and correspond to low deep-sea P accumulation rates, whereas glacially lowered sea levels allow for shelf bypassing and greater deep-sea P accumulation rates.

[1]Now at Amoco Production Company, Houston, Texas.

Paper number 7P0956.
0883-8305/88/007P-0956$10.00

INTRODUCTION

Phosphorus (P) is the limiting nutrient in the marine realm and consequently, the limiting factor to marine carbon fixation and burial. The present total riverine P flux to seawater is about 1.8×10^{12} g/yr [Lerman et al., 1975], yielding an ocean-wide steady state flux to marine sediments of about 0.5×10^{-6} g/cm^2/yr [Holland, 1978; Froelich et al., 1982]. Therefore the study of total P present in deep-sea sediments provides important information on the marine realm at the time of sediment burial.

In a conceptual model (Figure 1) of a steady state system the four most abundant biogenetic components of deep-sea sediments (C, $CaCO_3$, SiO_2, and P) enter the surface ocean in dissolved and/or organically complexed (and hence biologically

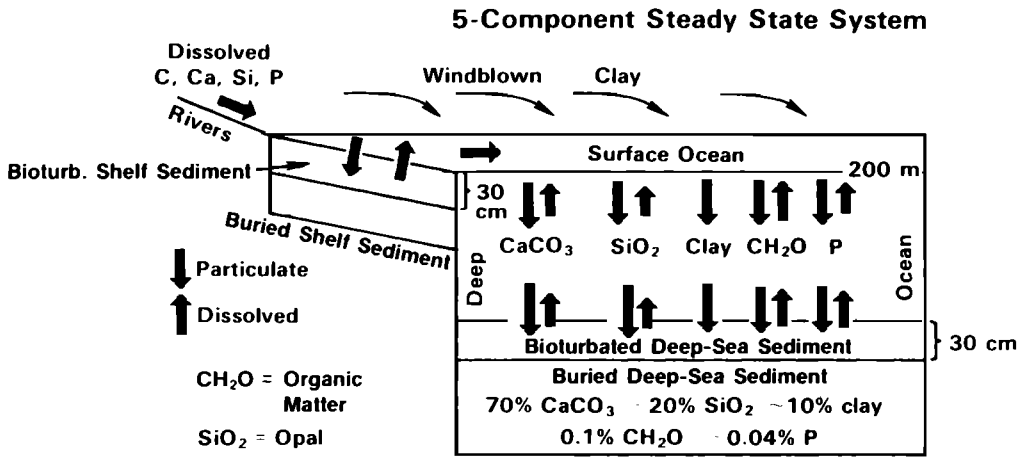

Fig. 1. Conceptual steady state representation of the five most common components ($CaCO_3$, silica, clay, organic matter, and P) of marine sediments.

useable) forms via rivers. These components immediately enter the marine biologic cycle to produce carbonate, opal, organic matter, and apatite. The fifth component, windblown terrigenous dust, does not participate in biochemical reactions and therefore serves only as a diluent to biogenic sediments.

As windblown dust is essentially a sample of chemically "average" continental crust, it contains ~1000 ppm of non-reactive P [Taylor, 1964] that does not participate in biochemical reactions. If an accurate estimate of biologically reactive P flux is desired, this terrigenous P must be accounted for and removed from the reaction P-flux calculations. Terrigenous P flux is very low in all but sites 62 and 266.

Phosphorus is a near ideal biologic productivity tracer because it is less soluble in deep-sea sediments than calcite and opal, the other major productivity tracers. Long-term deep-sea phosphorus accumulation rates were studied by Moody et al. [1981] and Froelich et al. [1982] with the goal of understanding the steady state biogeochemical cycling from continental runoff to sediment sink. The accumulation rate of phosphorus into phosphorite deposits was examined by Burnett [1974, 1977], Arthur and Jenkyns [1981], and Riggs [1984]. Phosphorus in the water column is reviewed in detail by Broecker and Peng [1982]. Biogenic opal accumulation for the Antarctic Ocean was investigated by Brewster [1977]. Ocean current studies on the upwelling of nutrients for Antarctic Ocean were detailed by Gordon [1971a, b]. Metal and biogenic accumulation rates, calculated for the central equatorial Pacific by van Andel et al. [1975], Leinen [1975], and Leinen and Stakes [1979], provide additional data on the sedimentation and productivity history of the region. Doyle et al. [1979], Prince et al. [1980], and Corliss and Hollister [1982] have studied the giant piston core (GPC-3, C/V Long Lines 44) in the North Central water mass and provide data on the lithology, sedimentation rates, and ichthyolith (fish teeth) chronology. Ichthyoliths found in the GPC-3 site and other similar areas were described by Doyle et al. [1979], Dunsworth et al. [1975], and Ramsey et al. [1976]. In addition, Kennett [1985] assembled and contributed to a complete volume on the Pacific Miocene ocean evaluating its geologic history.

The objective of this study was to measure the total P flux to deep-sea sediments using the downcore variations in the total P content for three open ocean water masses (Table 1) for the past 10 million years. Phosphorus concentrations at ~1-Ma intervals were measured in samples of the Pacific and Antarctic oceans from nine Deep Sea Drilling Project (DSDP) sites and one giant piston core (Figure 2). The weight percent of carbonate, opal, and terrigenous material were measured for comparison with variations in total P content. A steady state system

TABLE 1. Site Specific Data on the Cores Studied

Site	Location	Present Water Depth, m	Average Sedimentation Rate, m/Ma	Oceanic Water Mass*	Present Character of Water Mass	Present Productivity	Primary Lithology	Key References
62	01 52.02'N 141 56.03'E	2591	22	Central Pacific	above lysocline	high	nannofossil ooze	Winterer et al. [1971], Bronnimann and Resig [1971], Berger [1972], Moody et al. [1981]
65	04 21.21'N 176 59.16'E	6130	5	Central Pacific	below CCD†	high	radiolarian ooze	Menard [1964], Winterer et al. [1971], Riedel and Sanfilippo [1971], Berger [1972]
66	02 23.63'N 166 07.28'W	5293	5.5	Central Pacific	below CCD	high	radiolarian ooze	Winterer et al. [1971], Riedel and Sanfilippo [1971], Moody et al. [1981]
77	00 28.90'N 133 13.70'W	4291	13	Central Pacific	within lysocline	high	radiolarian/ nannofossil ooze	Hays et al. [1972], Jenkins and Orr [1972], Berggren and van Couvering [1972], Moody et al. [1981]
266	59 24.13'S 110 06.70'E	4167	30	Antarctic	below CCD	high	diatomaceous ooze	Hays et al. [1972], Ciesielski [1975], Brewster [1977]
310	36 52.11'N 176 54.09'E	3516	6	North Pacific	within lysocline	intermediate	nannofossil ooze	Larson et al. [1975], Bukry [1975]
463	21 21.01'N 174 40.07'E	2532	3.5	North Pacific	above lysocline	low	nannofossil ooze	Thiede et al. [1981], Muller [1981], Cepek [1981]
572	01 26.09'N 113 50.52'W	3893	13-60	Central Pacific	within lysocline	high	siliceous/foraminiferal-nannofossil ooze	Berger and Winterer [1974], Pisias and Prell [1985, 1986]
586	00 29.84'S 158 29.89'E	2207	40	Central Pacific	above lysocline	high	foraminiferal-nannofossil ooze	Berger [1972], Shafkin [1975], Initial Core Description (unpublished work, 1983)
GPC-3	30 19.09'N 157 49.04'W	5705	2.5	North Pacific	below CCD	low	red-brown clays	Doyle et al. [1979], Prince et al. [1980], Corliss and Hollister [1982]

*Central Pacific is equatorial, North Pacific is central water mass, and Antarctic is subpolar.
†CCD is carbonate compensation depth.

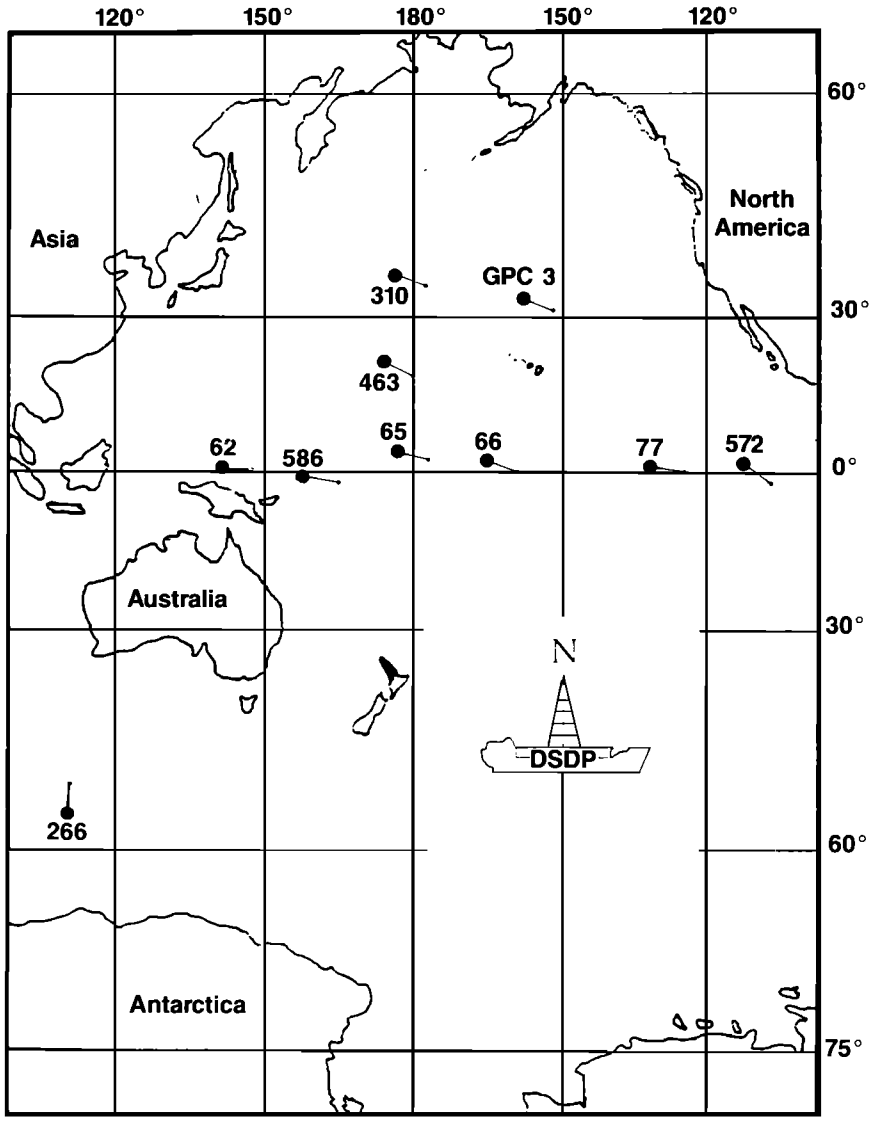

Fig. 2. The deep-sea site locations, their present (●) and 10 Ma (·) location defined by oceanic plate movement and water mass boundaries (central versus north Pacific).

was approximated because the oceanic residence time is 10^6 years for $CaCO_3$ and opal and 10^5 years for organic matter and P [Broecker and Peng, 1982]. These times are equal to or shorter than our ~1-Ma sampling intervals.

Paleoceanographic syntheses exist for the cores studied [Leinen, 1975; van Andel et al., 1975; Brewster, 1977, 1980; Doyle et al., 1979; Leinen and Stakes, 1979; Prince et al., 1980; Worsley and Davies, 1979; Moody et al., 1981; Davies and Worsley, 1981; Corliss and Hollister, 1982]. Global riverine inorganic and organic P supply to the marine realm has also been determined by Lerman et al. [1975], Meybeck [1982], Sandstrom [1982], and Smith [1984]. Therefore the effective determination and interpretation of the history of changes in accumulation rates of P and other productivity related components in deep-sea sediments, i.e., detailed climatic, physiographic, oceanographic, and plate tectonic characterization of the sites of deposition, are possible. In addition, a common time

scale to correlate the sites and a detailed history of the water mass changes overlying the sites are available.

Specific site locations (Figure 2) were chosen to provide information on biota burial flux changes with time for sedimentary sinks that include: (1) the equator above the lysocline, (2) the equator within the lysocline, (3) the equator below the carbonate compensation depth (CCD), (4) the central water mass above the lysocline, (5) the central water mass below the CCD, and (6) the subantarctic productivity belt near the CCD. In addition, other site selection criteria utilized in core selection included core quality, latitude, biogenic productivity, water depth, and lithology (Table 1). Biogenic and inorganic burial flux measurements calculated for these sites were then used to determine relationships between and among these sedimentary sinks to model total sedimentary output, thereby permitting improved estimates of burial fluxes through geologic time.

QUANTITATIVE METHODOLOGY

Sampling and Sample Preparation

Samples for this study were provided by Deep Sea Drilling Project core repository from sites 62, 65, 66, 77, 310, 463, 572, and 586. Samples from the C/V Long Line Cruise 44 site GPC-3 core were obtained from Woods Hole Oceanographic Institute. Crushed, homogenized samples from DSDP site 266 that had previously been analyzed for opal content were provided by Brewster [1977].

Accurate dating within a uniform absolute time scale was not available for the cores at the inception of this study. We therefore used the following procedure to obtain 1-Ma time slices down to approximately 10 Ma for each site. Forty samples were chosen at equal depth intervals downcore to a depth representing ~10 Ma. The spacing was dependent on the total core depth to the 10-Ma datum specified in the DSDP Initial Reports for each site. The downhole biostratigraphy for each individual sample was also obtained from the available DSDP reports for the sites. To date, many age-depth determinations for sites presented in the literature have been correlated to Berggren and van Couvering [1972] time scale. However, recent adjustments to the time scale amenable to nannofossil biostratigraphy were made by Haq [1983]. Sites 62.1, 65, 66, 77, and 266 therefore have been adjusted using the downhole correlation from Berggren and van Couvering [1972] to Haq [1983] time scale. Sites 310, 463, 572, and 586 were dated with nannofossil biostratigraphy by Worsley for this study (documented in Chaboudy, 1984). Site GPC-3 was dated by Prince et al. [1980] using paleomagnetics and by Doyle et al. [1979] using fish teeth. At the completion of plotting the standardized time scale age-depth plots for all samples, equal dry weight aliquots of 2-4 consecutive samples were combined into composite samples totaling 1 g for total P analysis [Chaboudy, 1984]. These composite samples (A1, A2, etc., Table 2) were specifically grouped to cover a 1-Ma time interval with an average depth for the mixed 2-4 samples. This physical mixing averaging procedure was used to reduce the number of total P analyses required for the wet chemical analysis of the silica-rich samples. Previous experience using single samples to represent 1-Ma intervals per core [Moody et al., 1981] also demonstrated the desirability of averaging samples over a specified time interval. One gram of each individual sample was saved for archival purposes.

The 1-g aliquots of each of the 1-Ma composite samples for the total P analysis were then disaggregated and homogenized using a carborundum mortar and pestle to obtain an approximately 300-mesh powder. Another uncrushed 1-g aliquot of the composite for the carbonate and biogenic opal was prepared by weighing into a beaker equal amounts of one-quarter to one-half g of each of the 2-4 samples representing each an approximate 1-Ma interval before analysis as was done for P analysis composite. This composite sample was not crushed because it would be used for the differential settling velocity grain size determination of the opal clay fraction after dissolution of the carbonate fraction.

Phosphorus Chemical Analysis

The total phosphorus analysis of the 0.125-g aliquots of the crushed 1-Ma composite samples was done exactly as reported by Moody et al. [1981] utilizing the same National Bureau of Standards (NBS) phosphate rock standard 120b for the P colorimetric standard curve [Chaboudy, 1984]. The 0.125-g aliquot was dissolved

TABLE 2. Phosphorus, $CaCO_3$, Biogenic Opal, and Terrigenous Sediment Contents, Age, and Accumulation Rates of all Sediment Components of DSDP Sites 62.1, 65, 66.1, 77, 266, 310, 463, 572, 586, and GPC-3

Site, Core, and Group Numbers	Sub-bottom Depth, m	Age, Ma	P, ppm	$CaCO_3$, wt %	Biogenic Opal, wt %	Terrigenous Sediment, wt %		P Accum. Rate, µg/cm²/ka	$CaCO_3$ Accum. Rate, g/cm²/ka	Opal Accum. Rate, g/cm²/ka	Terrigenous Accumulation Rate, g/cm²/ka		
						Fine	Coarse				Fine	Total	Coarse
						62.1							
1/2/66-70	8.0	0.2	790	59.0				1327	0.99			0.69	
3/1/142-146	25.0	1.0	542 (19)*	67.0				981	1.21			0.60	
A1†	45.0	1.8	430	75.9	0.12	11.90	12.20	1815	3.20	0.005	0.500		0.510
A2†	72.0	2.8	544	72.5	0.11	16.40	11.00	1485	1.98	0.003	0.450		0.300
9/3/66-70	85.0	3.2	734 (18)*	71.0				1923	1.86			0.76	
11/3/89-93	105.0	4.1	600	77.0				1542	1.98			0.59	
13/3/66-70†	123.0	4.6	717	84.0				2768	3.24			0.62	
15/3/65-69	142.0	5.1	486	77.0				1934	3.06			0.92	
A3†	158.0	5.6	344 (29)*	85.7	1.60	7.90	4.80	1290	3.21	0.060	0.300		0.180
19/3/72-76†	178.0	6.0	487	88.0				2260	4.08			0.56	
21/3/86-90	199.0	6.8	386 (1)*	87.0				1867	4.18			0.62	
23/3/64-68	220.0	7.1	445	79.0				2154	3.82			1.02	
25/3/87-91	238.0	7.6	386	88.0				1671	3.81			0.52	
27/3/63-67	258.0	8.0	387	85.0				1722	3.78			0.67	
29/3/64-68	275.0	8.6	332	86.0				1438	3.72			0.61	
						65.0							
B1†	2.5	0.8	3698	0.0	95.90	3.50	0.59	185	0.00	0.048	0.002		0.000
B2†	5.0	1.8	3287	0.0	95.90	3.50	0.61	99	0.00	0.029	0.001		0.000
B3†	7.0	2.4	3230 (32)*	0.0	92.40	7.00	0.60	420	0.00	0.120	0.009		0.001
1/5/80-84	8.0	2.6	2810	0.1				90	0.00			0.03	
2/2/80-84	12.0	3.4	2310	0.3				148	0.00			0.06	
2/5/88-92	17.0	4.6	2092	0.6				126	0.00			0.06	
3/2/88-92	21.0	5.2	2032 (62)*	0.7				256	0.00			0.13	
4/2/90-94	30.0	6.8	1956	1.3				483	0.00			0.25	
4/5/64-68	35.0	7.2	1942	1.5				388	0.00			0.20	
5/5/70-74	44.0	8.2	2072 (20)*	1.6				414	0.00			0.20	
6/2/86-90	48.0	8.6	2006 (45)*	1.0				439	0.00			0.22	
6/5/100-104	53.0	9.1	2095	0.5				459	0.00			0.22	
						66.1							
C1†	18.0	1.0	2067	0.0	91.00	7.90	1.03	537	0.00	0.240	0.021		0.003
C2†	23.0	2.2	1802	0.0	95.50	4.10	0.35	451	0.00	0.230	0.020		0.001
C3†	29.0	3.8	1090 (4)*	0.0	98.20	1.60	0.20	76	0.00	0.069	0.001		0.000
C4††	35.0	5.3	936	0.0	99.00	0.70	0.30	580	0.00	0.610	0.005		0.002
C5†	41.0	--	--	0.0	99.00	0.70	0.34	--	0.00	0.340	0.002		0.001
C6†	47.0	7.1	1359	0.0	99.30	0.70	0.00	313	0.00	0.230	0.002		0.000
C7†	53.0	--	--	0.0	98.30	1.50	0.30	--	0.00	0.170	0.002		0.001
C8†	59.0	10.0	1713	0.0	99.00	0.67	0.33	257	0.00	0.150	0.001		0.000

						77							
D1†	1.9	0.5	544	82.9	16.90	0.13	0.11	413	0.63	0.130	0.001		0.001
1/3/73-77	13.0	1.1	293	85.0				147	0.43			0.07	
2/3/72-76	23.0	1.6	487	80.0				1008	1.66			0.41	
4/3/74-78	40.0	2.8	601	69.0				1160	1.33			0.60	
7/3/74-78	68.0	5.1	294	82.0				215	0.60			0.13	
8/3/81-86	77.0	5.5	332	81.0				744	1.81			0.43	
9/3/76-80	86.0	5.7	390 (58)*	87.0				897	2.00			0.30	
10/3/70-74	95.0	6.1	295 (1)*	90.0				684	2.09			0.23	
12/3/60-64	113.0	6.8	291 (37)*	88.0				661	2.00			0.27	
13/3/76-80	123.0	7.0	330	85.0				749	1.93			0.34	
14/3/80-84	132.0	7.4	448	77.0				1017	1.75			0.52	
15/3/70-74	141.0	7.9	274 (18)*	89.0				630	2.05			0.25	
16/3/77-81	150.0	8.0	638	85.0				1289	2.02			0.36	
D2††	159.0	9.4	838 (10)*	82.3	17.50	0.06	0.12	1718	1.69	0.360	0.000		0.000
D3†	169.0	9.5	525	74.4	25.60	0.03	0.00	877	1.24	0.430	0.001		0.000
D4†	179.0	9.8	360	89.6	10.30	0.00	0.00	857	2.13	0.250	0.000		0.000
						266							
J1††	4.0	0.5	278	11.1	69.40	19.5		500	0.20	1.240		0.35	
J2††	23.0	1.3	360	2.3	64.00	33.8		572	0.04	1.020		0.54	
J3†	87.0	2.3	689 (6)*	2.0	38.70	59.2		1178	0.03	0.670		1.01	
J4††	113.0	3.5	474	1.8	53.50	44.7		953	0.04	1.070		0.90	
J5†	133.0	4.6	721	2.3	38.40	59.3		584	0.02	0.310		0.48	
J6†	141.0	5.4	582	2.1	38.40	59.6		355	0.01	0.230		0.36	
J7†	151.0	6.0	449	35.7	21.00	43.3		242	0.19	0.110		0.23	
J8†	156.0	7.2	563	36.4	11.80	51.8		315	0.20	0.070		0.29	
J9†	162.0	8.1	588	15.3	27.40	57.3		241	0.06	0.110		0.23	
J10†	166.0	9.6	866	1.3	28.00	70.7		251	0.00	0.080		0.20	
						310							
E1††	3.0	0.2	518	63.1	32.60	3.30	0.91	767	0.93	0.480	0.049		0.013
E2††	8.0	0.6	335	69.5	27.80	2.70	0.00	596	1.24	0.500	0.048		0.000
E3†	17.0	1.3	278 (19)*	82.4	14.70	1.50	1.40	514	1.52	0.270	0.027		0.027
E4†	24.0	1.7	284	86.8	7.80	0.86	4.60	521	1.59	0.140	0.016		0.083
E5†	30.0	2.1	--	86.2	11.00	0.58	2.30	--	1.34	0.170	0.009		0.035
E6†	37.0	2.6	272	89.7	8.80	0.68	0.87	539	1.78	0.170	0.013		0.017
E7†	43.0	3.1	252	91.0	7.20	0.14	1.70	305	1.10	0.087	0.002		0.021
E8†	49.0	3.8	367	72.4	19.50	6.30	1.80	422	0.84	0.230	0.073		0.021
E9†	56.0	4.5	398	80.3	14.10	4.70	1.00	362	0.73	0.130	0.043		0.001
E10†	63.0	5.6	563	77.0	11.40	11.40	0.10	715	0.98	0.150	0.150		0.001
E11†	70.0	6.9	487	83.5	7.20	7.20	2.10	185	0.32	0.027	0.027		0.008
E12†	76.0	9.2	721	80.0	3.90	15.60	0.52	231	0.26	0.013	0.050		0.001
						463							
F1†	2.0	1.2	588	82.9	0.00	11.60	5.50	106	0.15	0.000	0.021		0.010
F2†	4.0	2.0	506	88.4	0.00	7.90	3.70	460	0.80	0.000	0.072		0.034
F3†	7.0	2.9	401 (23)*	91.9	0.00	5.90	2.20	64	0.15	0.000	0.009		0.004
F4†	10.0	3.7	392	94.7	0.00	3.40	1.90	459	1.11	0.000	0.039		0.023
F5†	13.0	4.0	721	91.4	0.00	6.30	2.40	591	0.75	0.000	0.052		0.019
F6†	17.0	4.9	272	94.9	0.00	3.60	1.40	68	0.24	0.000	0.009		0.004
F7†	20.0	6.1	1056	90.7	0.00	6.70	2.70	222	0.19	0.000	0.014		0.006
F8†	23.0	8.4	348	90.6	6.50	0.71	2.20	219	0.57	0.041	0.004		0.014
F9†	27.0	9.8	651	95.5	0.53	3.80	0.16	91	0.13	0.000	0.005		0.001

TABLE 2. (continued)

Site, Core, and Group Numbers	Sub-bottom Depth, m	Age, Ma	P, ppm	$CaCO_3$, wt %	Biogenic Opal, wt %	Terrigenous Sediment, wt %		P Accum. Rate, $\mu g/cm^2/ka$	$CaCO_3$ Accum. Rate, $g/cm^2/ka$	Opal Accum. Rate, $g/cm^2/ka$	Terrigenous Accumulation Rate, $g/cm^2/ka$		
						Fine	Coarse				Fine	Total	Coarse
						572							
G1†	11.0	1.2	430	84.1	16.00	0.00	0.00	529	1.03	0.200	0.000		0.000
G2†	36.0	2.5	721	73.8	26.10	0.17	0.00	923	0.94	0.330	0.002		0.000
G3†	62.0	3.9	636 (10)*	73.0	27.00	0.00	0.00	1010	1.16	0.430	0.000		0.000
G4†	88.0	4.9	499	81.2	18.80	0.00	0.00	1647	2.68	0.620	0.000		0.000
G5	114.0	5.4	632	70.2	29.80	0.00	0.00	3267	3.63	1.540	0.000		0.000
G6†	143.0	5.9	499	80.2	19.80	0.00	0.00	3258	5.24	1.290	0.000		0.000
G7††	170.0	6.4	303	64.8	35.20	0.00	0.00	1336	2.86	1.550	0.000		0.000
G8†	196.0	6.9	455	73.0	27.10	0.00	0.00	1775	2.85	1.050	0.000		0.000
G9†	221.0	7.7	405	74.7	25.30	0.00	0.00	944	1.74	0.590	0.000		0.000
G10†	251.0	9.7	442	78.3	21.70	0.06	0.00	760	1.35	0.370	0.001		0.000
						586							
H1†	20.0	0.8	436	91.6	4.80	3.10	0.57	1134	2.38	0.12	0.080		0.015
H2†	53.0	2.1	695	92.2	4.20	3.30	0.29	2641	3.50	0.16	0.130		0.011
H3†	86.0	3.3	386 (32)*	93.9	4.40	1.60	0.14	1594	3.88	0.18	0.067		0.006
H4†	118.0	4.3	329	94.8	1.90	2.80	0.47	1497	4.31	0.09	0.130		0.021
H5†	150.0	5.1	379	93.8	5.00	0.48	0.72	1766	4.37	0.23	0.022		0.034
H6†	181.0	5.8	335	96.9	2.70	0.00	0.44	2030	5.87	0.16	0.000		0.027
H7†	212.0	6.5	247	95.9	3.30	0.00	0.83	1771	6.88	0.24	0.000		0.060
H8†	243.0	7.3	190	95.9	3.60	0.00	0.50	1102	5.56	0.21	0.000		0.030
H9†	275.0	8.2	221	94.7	4.30	0.00	1.03	1076	4.61	0.21	0.000		0.050
H10††	298.0	8.9	158	90.4	8.50	0.00	1.11	978	5.60	0.52	0.000		0.070
						GPC-3							
I1†	0.3	0.2	790	0.0	0.00	71.60	28.40	237	0.00	0.00	0.220		0.085
I2†	1.1	0.5	853	0.0	0.00	72.70	27.30	222	0.00	0.00	0.190		0.074
I3†	1.9	0.9	756 (10)*	0.0	0.00	71.00	29.10	143	0.00	0.00	0.140		0.052
I4†	2.7	1.3	745	0.0	0.00	74.80	25.20	134	0.00	0.00	0.130		0.052
I5†	3.5	1.8	898	0.0	0.00	71.70	28.30	135	0.00	0.00	0.110		0.042
I6†	4.3	2.3	973	0.0	0.00	65.20	34.80	97	0.00	0.00	0.065		0.035
I7†	5.1	3.1	1169	0.0	0.00	62.80	37.20	82	0.00	0.00	0.044		0.026
I8†	5.9	4.9	1378	0.0	0.00	63.90	36.10	41	0.00	0.00	0.019		0.011
I9†	6.8	8.4	1884	0.0	0.00	71.00	29.00	38	0.00	0.00	0.014		0.006

Total sediment accumulation rate = $CaCO_3$ + opal + terrigenous accumulation rates; carbonate-free accumulation rate = opal + terrigenous accumulation rates.

*Range from duplicate analyses (in parts per million).

†These samples show the 2 to 3 and 5 to 6-Ma peaks in accumulation rate versus time or exhibit high opal content, or have undergone an equatorial crossing.

†Composite samples for ~1-Ma time interval; exact DSDP individual sample numbers are available from the authors or Chaboudy [1984]; subbottom depths are an average from 2 to 4 individual samples; age was determined from the nannofossil biostratigraphy utilizing the Haq [1983] time scale.

Accum. = Accumulation.

using both concentrated HCl and HF in a modified Bernas procedure [Bernas, 1968]. The total P concentration for the unknown solutions was determined colorimetrically after the method of Shapiro [1975] from a standard curve prepared from NBS rock standard. Duplicate P analysis of samples from each site are shown in Table 2. The largest errors of 7-16% occurred in those samples with total P concentrations <400 ppm. Samples with P concentrations >500 ppm had 3% or less error. The single sample P analyses, e.g., site 62, 1/2/68-70, are those reported by Moody et al. [1981].

Carbonate, Biogenic Opal, and Clay Measurements

Percent carbonate values were determined by acid dissolution of the uncrushed 1-g composite aliquot with 10% reagent grade HCl by weight difference after dissolution. Replicate measurements yield 3% standard deviation in carbonate measurements [Chaboudy, 1984]. Percent opal and clay were estimated from the carbonate determination residues using a simple settling velocity technique [Jackson, 1979] based on the assumption that nonbiogenic silica (quartz and clay mineral grains) are derived from wind transport and fall below the 5.0-μm size fraction, whereas the majority of biogenic silica material resides in the >5.0-μm fraction. Visual estimates of mineral/opal ratios from smear slides prepared from both the coarse and fine fractions from the above setting velocities were then used to adjust the settling velocity size determinations (see Chaboudy [1984] for a detailed technique description). The percent mineral/opal measurements are not intended to render values as precise as Leinen [1975] and Brewster [1977] but rather to produce first-order estimates of downhole accumulation rate trends relative to other deep-sea constituents, i.e., P, $CaCO_3$, and total sediment. The combined settling velocity/visual estimates adjustment technique is good to within ±10% for the few values in common with those of Leinen [1975] and Leinen and Stakes [1979] for site 77, which were determined in this study also.

We chose not to measure organic C content because this carbon type invariably degrades to the same low values (0.1-0.2 wt %) for all Pacific Ocean deep-sea sediments regardless of delivery rate to the seafloor and hence does not provide very useful ocean productivity information. Heath et al. [1977] have shown that deep-sea organic carbon content almost invariably decays to such values by the time they are buried to a depth several tens of meters, despite values approaching 5% for surface sediments under the richest productivity belts. However, the effect of initial organic matter concentrations near the sediment water interface on other biogenic components may be significant. Organic material oxidizing on or near the seafloor releases CO_2 and P. The CO_2 accelerates the dissolution of pH-sensitive $CaCO_3$ but not of the less pH-sensitive opal. The regenerated P refluxes in part to seawater, but a significant fraction renucleates and is buried as apatite [Moody et al., 1981; Sandstrom, 1982].

Depositional Component Accumulation Rates

Sedimentation rates used in calculating accumulation rates are based on age-depth interpretations from downhole biostratigraphic determinations discussed earlier [Chaboudy, 1984]. Then sediment accumulation rates (mass of sediment/unit area/unit time) are calculated for uniform subbottom depth intervals for the past 10 Ma at each location for total sediment, carbonate ($CaCO_3$), carbonate-free (residual), and total phosphorus (P). The carbonate-free fraction is subdivided into opal and nonbiogenic (fine and coarse) fractions. Wet bulk density and porosity data (obtained from DSDP core repository for each specific core sample) are used to subtract the mass of seawater in the wet cores, thereby allowing sediment accumulation to be expressed in terms of mass/unit area/unit time when combined with the age-depth relationships. The accumulation rate for each component can then be calculated utilizing the derivation of van Andel et al. [1975]. Usage of the Haq [1983] time scale results in slightly different calculated accumulation rates for sites 62.1, 65, and 77 than were reported by Moody et al. [1981], and those rates were adjusted accordingly for use in this study (Table 2).

RESULTS

The results of this work will be discussed with respect to two important aspects of marine sedimentation: (1) com-

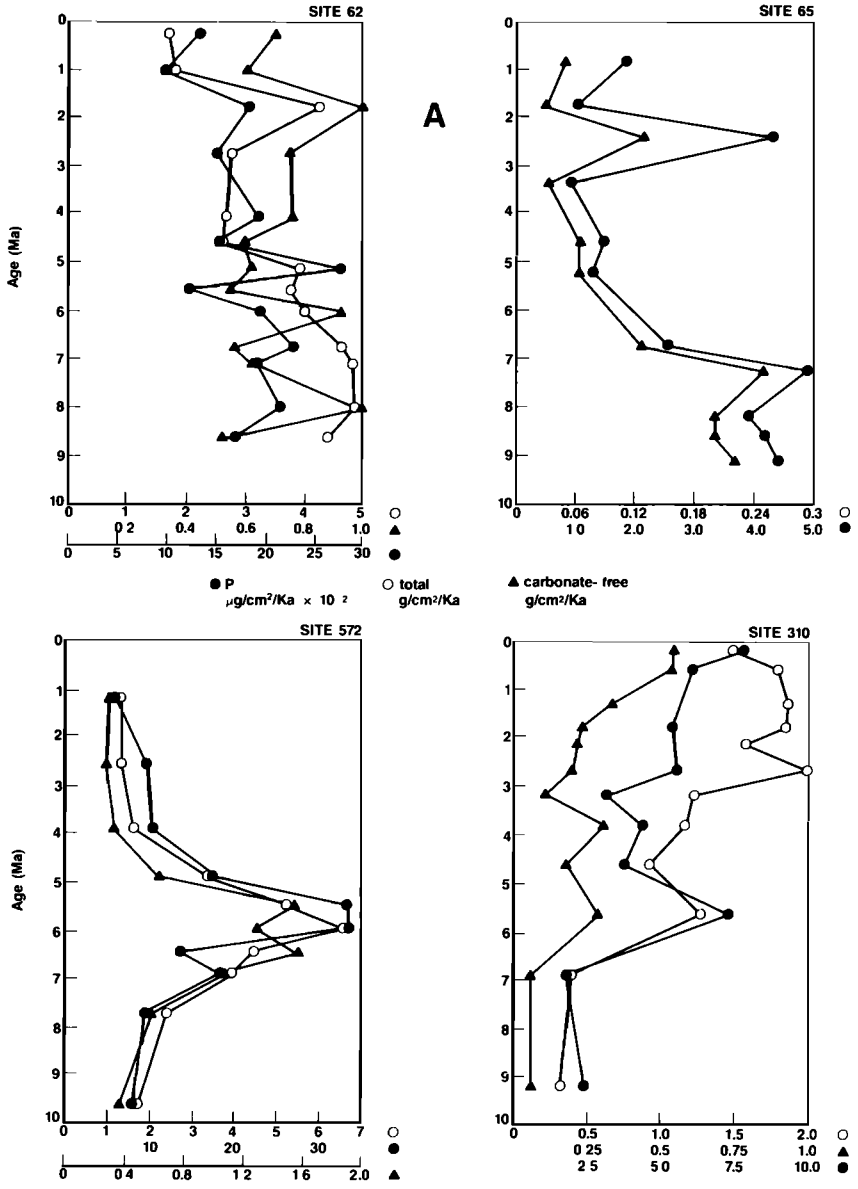

Fig. 3a. Phosphorus, total sediment, and carbonate-free accumulation rate versus age (Ma) for sites 62, 65, 572, and 310.

ponent flux variations for the last 10 m.y. and (2) individual characteristics of site accumulation rates. These marine sedimentation results will also be related to the major biota burial flux changes with time.

Accumulation Rates for the Last 10 m.y.

Variations in the accumulation rates of total P, total sediment, carbonate-free, $CaCO_3$, and opal have been determined for the last 10 m.y. Data are presented to contrast P, total sediment, and carbonate-free components within individual sites (Figure 3A, B, C). Chaboudy [1984] also plotted $CaCO_3$ and opal accumulation rates for individual sites, and a series of contour maps were drawn showing the areal distribution of P accumulation rates through time for the north-central and central equatorial Pacific.

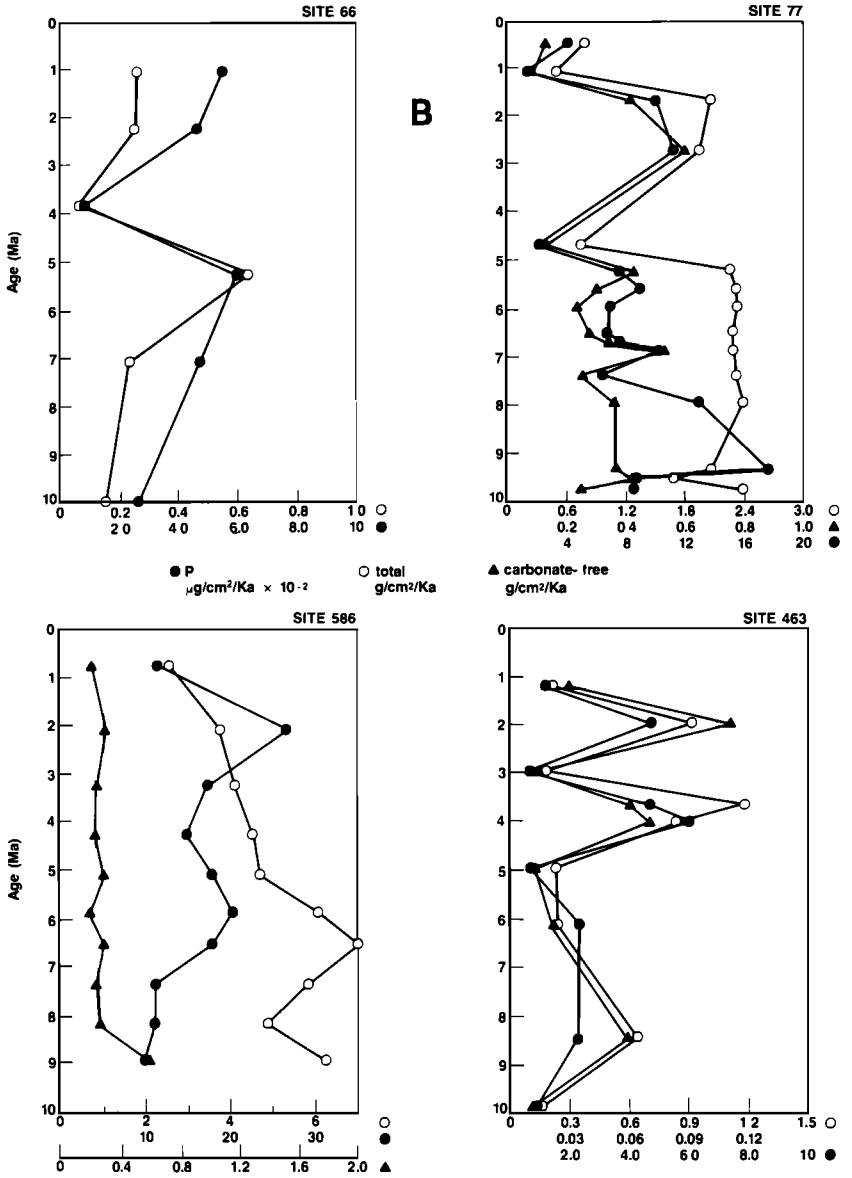

Fig. 3b. Phosphorus, total sediment, and carbonate-free accumulation rate versus age (Ma) for sites 66, 77, 586, and 463.

The accumulation rate versus time results of Moody et al. [1981] are based on single samples spaced at approximately 1-Ma intervals. Experience with that procedure suggested that the sampling interval was too coarse to define accumulation rate peaks accurately. Therefore the peaks determined from our present sampling procedure are more reliably characteristic of deep-sea sediment accumulation rates. However, the measurements of Moody et al. [1981] are still used after recalibration to the Haq [1983] time scale and are augmented by newly analyzed composite samples as necessary to fill in time gaps (Table 2) for sites 62.1, 65, and 77, specifically.

Figure 3 shows that each site displays downhole variations of at least a factor of 2 for each of the components through time, but they do not always covary within any site. Similarly, inspection suggests

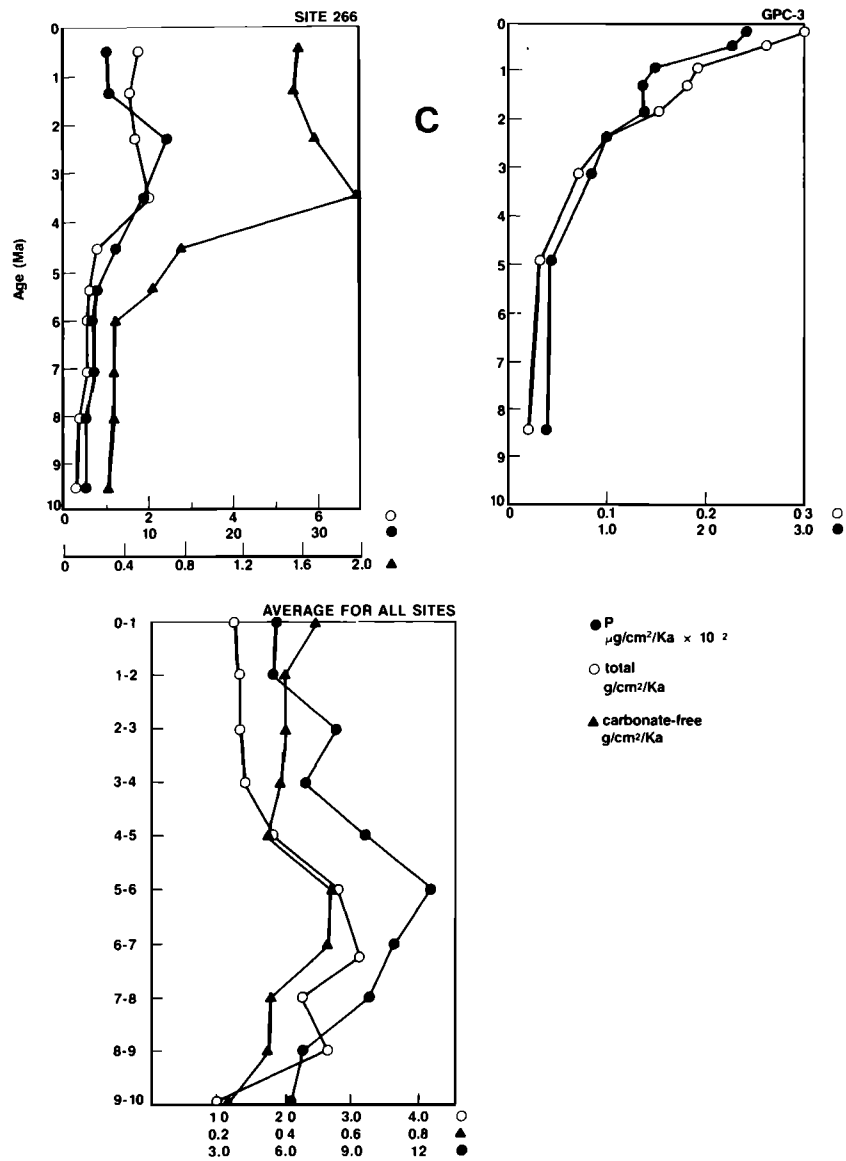

Fig. 3c. Phosphorus, total sediment, and carbonate-free accumulation rate versus age (Ma) for sites 266, GPC-3, and average for all sites (Figures 3a, 3b, and 3c).

that some, but not all, peaks and troughs in component accumulation rates appear to be coeval among sites where they co-occur but that none are detectable at all sites. Figure 3C also contains a plot of accumulation rates for the three components arithmetically averaged for all sites. Biogenic component accumulation rates at a site change through time as either a function of global changes in runoff-supplied solutes ($CaCO_3$, SiO_2, P) or as a result of the site's migration into or out of productivity belts. The former will tend to be coeval among sites, whereas the latter will be site specific. None of the Pacific sites chosen for study were involved in ridge-crest processes during the last 10 m.y. Figure 4 was drawn as an interpretive summary of the P peaks observed for all 10 sites. The phosphorus accumulation rate for the entire data set is characterized by two prominent peaks

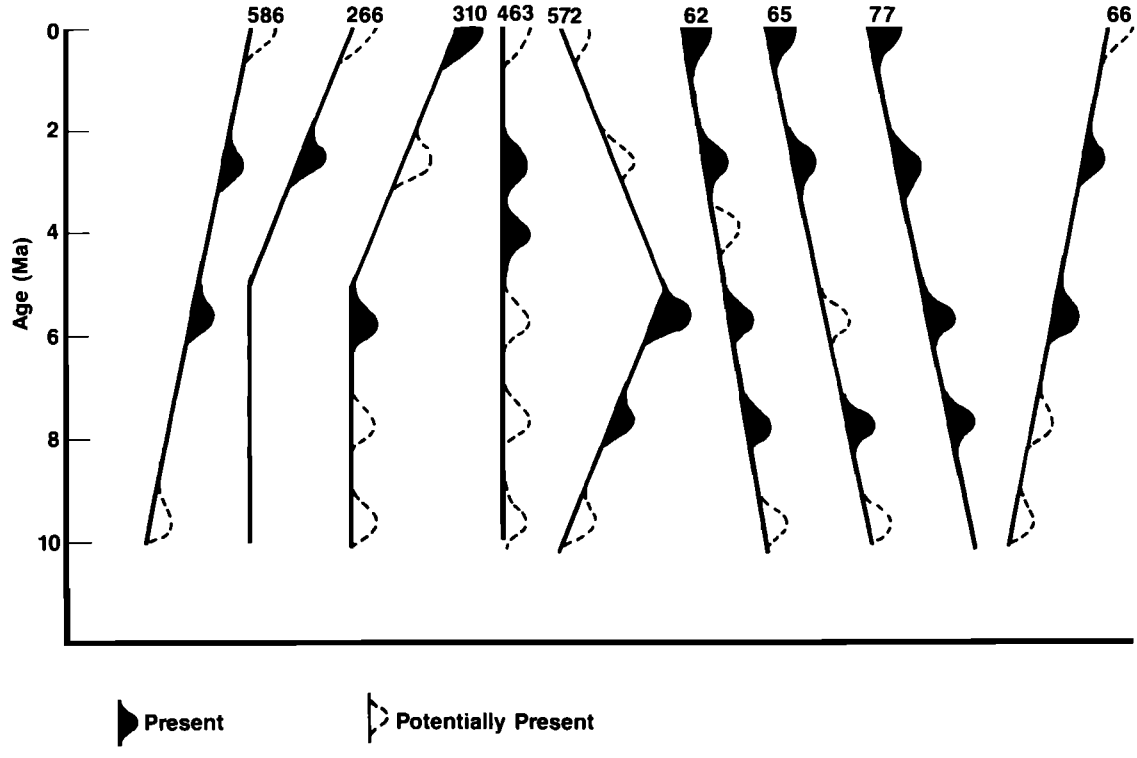

Fig. 4. Conceptual interpretation of P accumulation rate peaks as present and/or potentially present in last 10 Ma for the cores studied. A potentially present peak is one that may be revealed by subsequent sampling and analysis. Slant upward to the right shows P accumulation rate increasing as the sites move toward the equator or a known productivity belt. Slant upward to left specifies the opposite. Filled in peaks represent those clearly present in data, and dashed peaks are possibly present but cannot be resolved within the current sampling interval. The peaks are schematically superimposed upon secular trends and adjusted to be synchronous within the constraints provided by the sampling interval.

at 5-6 Ma and 2-3 Ma (Figure 3) with the 5-6 Ma peak being the larger. The time intervals characterized by peaks in the accumulation rates (Figures 3 and 4) will be identified and discussed next.

A P peak centered on 7-8 Ma occurs in equatorial sites 62, 65, 77, and 572 and is possibly present in sites 66, 310, and 463 (Figures 3 and 4). This P peak's significance is not known at this time; it corresponds to no known major paleoceanographic event, except perhaps a shoaling of the CCD [Heath et al., 1977]. On the average P accumulation rate curve for all sites (Figure 3C), the 7- to 8-Ma peak shows as a shoulder of the very large peak centered on 5-6 Ma and hence could be a sampling/dating artifact.

A sharp increase in P flux occurs at 5-6 Ma at all sites but 65, 463, 266, and GPC-3 (Figures 3 and 4). This peak is by far the dominant peak in the average of all the data sets and appears to be closer to 6 Ma than 5 Ma (Figure 3C). This increase can be related to significant changes in the deep-sea circulation and upwelling patterns [Bender and Keigwin, 1979; Barron et al., 1986] and consequently, to atmospheric circulation patterns. These changes include an increase in biogenic opal accumulation in the southern [Brewster, 1977] and equatorial [Leinen, 1975] Pacific oceans, sharp eustatic regression [Haq et al., 1987], and a shoaling of the Pacific CCD because by the middle of the upper Miocene

the flow of newly formed north Atlantic deep water moved toward the north Pacific [Berger, 1972; van Andel et al., 1975; Heath et al., 1977; Bender and Graham, 1978]. In addition, an increase in global precipitation rates and corresponding increase in Antarctic ice volume is suggested by the increase in foraminiferal $\delta^{18}O$ [Kennett et al., 1979]. The $\delta^{13}C$ [Kennett et al., 1979] ratio shows a negative excursion for this interval, indicating some change in the Pacific deepwater environment and perhaps caused by an exchange with some portion of the total ocean reservoir [Vincent et al., 1980]. A significant increase in explosive volcanism [Kennett et al., 1979] at this time probably enhanced the nonbiogenic P flux to the seafloor (~1050 ppm P crustal abundance; Taylor [1964]) but more importantly served to enhance global precipitation, and hence dissolved P runoff from the continents whose emergent area was then increasing owing to sea level fall caused by increased Antarctic ice accumulation.

At 2-3 Ma a peak occurs in the P accumulation rate curves for 8 of the 10 sites and possibly in those for the other two (310 and 572). The P accumulation peak is well resolved in Figures 3 and 4 and clearly corresponds to the establishment of northern hemisphere ice sheets [Haq et al., 1987]. Also, the 2- to 3-Ma P spike corresponds well to an increase in foraminiferal $\delta^{18}O$ [Kennett et al., 1979], which has been attributed to the onset of plio-Pleistocene northern hemisphere glaciation that affected both water temperature and ice sequestering of $\delta^{18}O$. Glacial onset has been linked to high marine productivity because periods of glaciation increase latitudinal temperature gradients that in turn cause increased upwelling of nutrient-laden bottom waters, resulting in planktonic proliferation [Kennett et al., 1979]. However, upwelling changes alone cannot increase the "long-term" global P flux to deep-sea sediments because the accumulation rate of P would increase under upwelling areas only at the expense of other areas. Therefore the most important factor affecting long-term ocean-wide P flux is continental runoff. During initiation of a glacial interval, increased precipitation would yield increased runoff and hence add dissolved phosphorus to the oceanic system which inevitably (residence time ~10^5 years; Broecker and Peng [1982]) becomes part of the deep-sea sediment record. However, establishment of ice sheets would serve to decrease aqueous runoff and again decrease riverine P input to the sea [Worsley et al., 1986]. These trends are suggested by the coincidence of P accumulation peaks between sample sites (Figure 4).

Finally, a 0- to 1-Ma P peak occurs in sites 62, 65, 77, and 310 (Figures 3A, 3B, and 4). This peak requires better characterization but appears to correspond to an interval of intense northern hemisphere glacial intervals and concomitant lowered sea levels [Haq et al., 1987]. It is not resolved in the averaged value for all 10 sites (Figure 3C).

All other changes in component accumulation rates are water mass, or site specific, and can be related to the relative migration between the site and a productivity belt. Each individual site will now be discussed utilizing the results from this study and all available information on the specific site.

Site 62. The westernmost part of the central equatorial upwelling zone is represented by site 62 located north of New Guinea (Figure 2). The terrestrial influence of this island arc, e.g., volcanics, is responsible for the "noisy" signal and apparent lack of component correlation [Chaboudy, 1984]. This problem, reported by Moody et al. [1981], well illustrates that the accumulation of continental detritus can mask the trace biological signals. However, the 2- to 3-Ma spike (Figures 3A and 4) is still evident, indicating that this glacial event must have been very prominent.

Site 65. This site has a pronounced P spike at 2-3 Ma (Figures 3A and 4) corresponding to the above-described glacial event. The P peak at 7 Ma is probably related to the 5- to 6-Ma event, given the inherent inaccuracies of dating this particular site [Riedel and Sanfilippo, 1971]. Also, "aliasing" from sparsely sampled data [Pisias and Prell, 1985] could extend the 7-Ma peak up into the 6-Ma ($\pm$0.75 Ma) interval. The high P content in the samples for this site and site 66 (Table 2) is directly related to the fact that both sites are below the CCD and in areas of high productivity. The P originally present in the organic material and calcite is now directly associated with biogenic silica because of dissolu-

tion of the carbonate and oxidation of the organic fraction originally present in the sediment.

Site 66. The sampling interval for site 66 is inadequate; sample "aliasing" is therefore a potential problem for an accurate interpretation of the activity of sedimentary components. P accumulation peaks can be seen at 2-3 Ma and 5-6 Ma (Figures 3B and 4) corresponding to the above-mentioned glacial events. The sharp drop in P and total sediment accumulation rates at 4 Ma is the result of an unconformity which is evident from the sedimentation rate plots of Chaboudy [1984]. Since both P and total sediment accumulation rates parallel one another at 4 Ma, the unconformity is probably caused by a drop in sedimentation rate rather than erosion or dissolution. Erosion by bottom currents has a tendency to concentrate apatite but not organic P because phosphate minerals have a high density and will lag as the lighter material is winnowed. Dissolution and reprecipitation also tends to increase P content of sediments because phosphate minerals are insoluble compared to calcite as noted above for site 65 and this site.

Site 77. The time interval from 5.5 to 10 Ma for this site is characterized by P and carbonate-free accumulation rates inversely related to the total sediment and $CaCO_3$ accumulation rates, which is not understood. This inverse relationship may be an indication of the amount of organic carbon oxidizing within the sediment prior to permanent burial. The actual production of organic carbon in the pelagic realm through time is not well known [Broecker and Peng, 1982]. In oceanic sites with high total sediment accumulation rates but near CCD, e.g., site 77, fluctuations in opal accumulation give a truer picture of productivity than fluctuations in carbonate accumulation [Leinen and Stakes, 1979; Brewster, 1980]. Even though opal is more soluble than carbonate in the deep sea [Heath, 1974; van Andel et al., 1975], its solubility, unlike that of calcite, is water depth independent. Hence opal, unlike calcite, can preserve well under adequate burial rates at all water depths and be less affected by CO_2 released from the dissolution of organic material. Therefore a high flux of organic material that oxidizes near the sediment-water interface would tend to reflux carbonate back to seawater via CO_2 dissolution while not affecting opal preservation. The P that parallels opal accumulation rate results from phosphorus precipitating in the sediment after carbonate and organic material are removed.

From 5.5 Ma to the present (Figure 3B, Table 2), carbonate and total sediment accumulation parallel P and opal (2- to 3-Ma spike is very prominent), indicating less organic material reaching the seafloor to oxidize and therefore dissolve carbonate. It is unclear why organic material could behave differently at site 77 in these two time periods. However, the 6-Ma late Miocene/early Pliocene event has been well documented as a time of reorganization in global oceanic circulation [Barron et al., 1985, 1986], which could partially explain the change in the chemical response to organic material.

Site 310. Hess Rise has a unique depositional history because it has straddled the north central water mass and the northern opal belt [Larson et al., 1975]. As site 310 migrated to the northwest (Figure 2) as a result of seafloor spreading, the small total sediment accumulation rates (<0.5 $g/cm^2/ka$; Table 2), characteristic of central gyre sedimentation, were progressively replaced by the much higher burial rates (1.0-2.0 $g/cm^2/ka$) reflecting the opal belt productivity. Superimposed on the secular P increase from 10 Ma to the present attributable to site migration are the two glacial onset spikes at 2-3 and 5-6 Ma (Figures 3A and 4). Concurrent with the 2-Ma northern glaciation is a decrease in carbonate and total sediment accumulation rates which continues to the present, marking the beginning of opaline dominance. The phosphorus accumulation trend for site 310 is an effective tracer of the productivity history of the surface ocean water.

Site 572. The high sedimentation rate at this fairly shallow water site with high percentages of biogenic components in pristine condition (<6 Ma; Pisias and Prell [1985, 1986]; and Barron et al. [1986]) makes site 572 an excellent candidate for exploring the interrelationships between trace element accumulation and surface biota activity. The history of eastern Pacific equatorial productivity for site 572 is marked by an extremely large increase in all sedimentary components between 8 and 4 Ma, with a peak at 6 Ma (Figure 3A). This "bloom" in produc-

tivity is attributed to site migration across the center of the equatorial upwelling zone at the exact time of the 5-6 Ma onset of southern hemisphere ice volume increase. P accumulation takes on a trend strongly parallel to those of all the other biogenic components. The extremely strong downhole covariation of all biogenic components suggests that site 572 may represent the most pristine record of surface water history in the equatorial Pacific.

Site 463. Site 463 is located in the mid-Pacific mountains within the north central Pacific water mass and is characterized by low sedimentation rates (~3.5 m/Ma; Thiede et al. [1981]). Site 463 was chosen to represent deep-sea sedimentation above the CCD in an area with low productivity. In making an estimate for the average areal distribution of phosphorus for the last 10 m.y. this site is very important. As with any depositional site with a low sedimentation rate, absolute dating becomes difficult, and the problems are amplified by unrecognized slumps off the flanks of this mountainous site. The sedimentation curve of Chaboudy [1984] documents some slumps and suggests potential for more. The component accumulation increase at approximately 4 Ma (Figure 3B) may therefore represent only the slump-disrupted remains of a very fragmentary record. Lack of a more suitable site with which to study a sterile, terrigenous-free, relatively shallow environment mandated use of site 463.

Site 586. Phosphorus deposition at site 586 shows a generally increasing trend from 9 to 1 Ma (Figure 3B). Superimposed are the two glacial events at 5-6 and 2-3 Ma. Carbonate and total sediment accumulation data exhibit a strong increase at the 5- to 6-Ma event but generally decrease toward the present. Opal and carbonate-free accumulation decrease with time at a much lower rate. The increase in P flux with time is an indication of increased calcite and organic carbon P transport to the seafloor. The insoluble P lags in the sediment as both carbonate and organic carbon are refluxed. An increase in P flux gradient between sites 586 and 65 in the time intervals 5-6 and 3-4 Ma has been shown [Chaboudy, 1984]. During the 5- to 6-Ma interval, P flux increases at site 586 as a result of the 5- to 6-Ma glacial event.

Site 266. During the late Miocene/early Pliocene, a major expansion of the Antarctic ice sheet occurred [Mayewski, 1975; Kennett et al., 1979], marking the northward shift of the siliceous productivity belt to approximately the southeastern Indian Ridge [Kemp et al., 1975]. Increases in component flux (Figures 3C and 4) are easily seen and agree well with biogenic silica and bulk accumulation data reported by Brewster [1977]. Phosphorus accumulation rates increase steadily from 5.5 to ~2 Ma, reacting to both the Antarctic and northern glaciation. In parallel, the P accumulation trend from 3.5 to 0.5 Ma is a carbonate-free track with an opposite opaline response. Productivity in the southern ocean, however, is not under the same constraints as in the Pacific equatorial region. Nutrient fluxes to surface waters are not the only factor limiting biogenic proliferation. The availability of sunlight [Brewster, 1977] also has a primary role in controlling rates of biotic activity.

Site GPC-3. Samples from site GPC-3 in the center of the north central Pacific gyre (Figure 2) were obtained in order to calculate the average background levels of phosphorus accumulation for the last 10 Ma. Sedimentation rates [Chaboudy, 1984] are based on ichthyolith [Doyle et al., 1979] and magnetic reversal stratigraphy [Prince et al., 1980]. Time intervals of 1 m.y. are very difficult to determine at this site because of core disturbance and extremely slow sedimentation rates (<1 m/Ma). A small increase in P flux exists at ~2 Ma (Figure 3C), but it is within the tolerance of analytical error. No increase is seen at 5-6 Ma. A gradual increase in P accumulation and total accumulation rates toward the present is probably the result of increased terrigenous sedimentation owing to the onset of northern hemispheric glaciation [Worsley and Davies, 1979].

From the above it is evident that secular changes in P accumulation as well as in other component accumulation rates, on both an averaged and site-by-site basis, record late Neogene paleoceanographic events the existence of which was previously inferred from other paleontological and geochemical information. Furthermore, these time series offer clues as to how P has participated in these events. However, the component accumula-

TABLE 3. Summary of Modern Day P Burial Fluxes and Accumulation Rates to Deep-Sea Sediments

	Froelich [1982]		Mach et al. [1987]	
	10^{-9} mol/ cm^2/yr	$\mu g/cm^2/ka$	10^{11} g/yr	$\mu g/cm^2/ka$
organic phosphorus	4	128	6	166
phosphorites	<1	<32	6†	166†
P in (Fe, Mn) coatings on $CaCO_3$*	4	128	3	83
metalliferous sediments	1.1	35	--	--
fish debris	<0.2	<6.4	--	--
total	<10.3	<329.4‡	15	415‡

*Palmer [1985] and Sherwood et al. [1987].
†Fluorapatites (both phosphorite and fish debris); apatite formation in modern marine sediments also noted by Jahnke et al. [1983].
‡Meybeck [1982] total dissolved inorganic and organic P was 276 $\mu g/cm^2/ka$.

tion rate information must be augmented to explain the specific mechanisms responsible for imprinting the evidence of these changes upon the sedimentary record. For revealing these mechanisms we now turn to the information gleaned by comparing the ratios of the accumulation rates of key components to each other in a time-independent framework on a site-by-site basis in order to understand how they relate to each other and especially to P.

CONTINENTAL-SHELF-DEEP-SEA PARTITIONING FOR THE LAST 10 M.Y.

Global Riverine P Flux to Deep Sea

Reactive phosphorus entering the ocean from riverine transport arrives as organic or inorganic material in dissolved or particulate form (Table 3). Recent work [Palmer, 1985; De Lange, 1986; Sherwood et al., 1987; Mach et al., 1987] has shown that P associated with biogenic $CaCO_3$ is found within iron manganese coatings and P is not incorporated into carbonate minerals. In addition, apatite crystallization from seawater [Gulbrandsen et al., 1984] and formation in upper sediment/ocean water interface [Jahnke et al., 1983; Krom and Berner, 1981; Jahnke, 1984] has been directly observed. Organic P and phosphorites (apatites and fish debris) are other major components in deep-sea sediments. A minor amount of P can also be provided by metalliferous sediments from mid-ocean ridge processes. The present total P accumulation rate to deep-sea sediments ranges from 276 to 415 $\mu g/cm^2/ka$. Table 4 shows that some sites for other specific geologic times had P accumulation rates less than this modern day burial flux, whereas the same sites at different geologic times had greater than modern-day P accumulation rates. These accumulation rate variations are directly related to specific site differences in productivity and the character of the water mass (see Table 1) which have changed as functions of time and plate position over the last 10 m.y.

The amount of phosphorus actually available to the deep sea for biogenic growth and reproduction is not accurately known. However, certain facts can be assumed concerning the amount of riverine P accumulating in deep-sea sediments. The quantity of riverine P considered "available" for biogenic use will range between dissolved P only and dissolved P with organic or inorganic particulate P. The numerical calculation of riverine P available for biogenic uptake within the equatorial and north Pacific productivity regimes are strongly dependent upon which P influx value is used. For this study two initial values for P influx were used (Table 5). Lerman et al. [1975] calculation of the P influx is used as a low value and Meybeck [1982] is used as a high

TABLE 4. Comparison of Site P Accumulation Rates (Table 2) to Froelich et al. [1982] Total Present-Day P Burial Flux of ≤329 μg P/cm^2/ka

Sites	Greater Than*	Sites	Less Than†
62.1	0.3-8.6 Ma	--	
65	6.7-9.2 Ma	65	0.8-5.3 Ma
66.1	1.1-2.2, 5.3 Ma	66.1	3.8, 7.1-10.0 Ma
77	0.5, 1.6, and 2.8, 5.5-9.8 Ma	77	1.1 and 5.1 Ma
266	0.5-5.4 Ma	266	6.0-9.6 Ma
310	0.2-2.6, 3.8-5.6 Ma	310	3.1, 6.9-9.2 Ma
463	2.0, 3.7, and 4.0 Ma	463	1.2, 2.9, 4.9-9.8 Ma
572	1.2-9.7 Ma	--	
586	0.8-8.9 Ma	--	
		GPC-3	0.2-8.4 Ma

*These sediments have a P accumulation rate >329 μg P/cm^2/ka.
†These sediments have a P accumulation rate <329 μg P/cm^2/ka.

value. The actual percentage of global riverine P permanently buried in either the equatorial or north Pacific is reported here as a range between these high and low values. Table 5 summarizes the calculations of the riverine P influx to the deep sea, which results in 17.6% [Lerman et al., 1975] and 3.6% [Meybeck, 1982] for both the equatorial and north Pacific areas. Therefore the P influx to reach these Pacific areas is roughly correlated to the riverine input, as well as to other key variables, i.e., location of a specific site, CCD, lysocline.

Glacial Intervals and Secular Changes in P Accumulation

Our results clearly show that P accumulation rate through time in the intermediate and deep Pacific Ocean is characterized by two prominent peaks centered on 5-6 and 2-3 Ma. These two peaks correspond to rapid buildup in the Antarctic ice sheet and northern hemisphere ice, respectively. In both cases, onset of ice buildup lowered sea level, increased the pole to equator thermal gradient, and consequently, simultaneously increased P input to the deep sea and increased the intensity of upwelling in the productivity belts. The P accumulation rate peak at 5-6 Ma is by far the larger and also represents a peak in total, carbonate-free, and carbonate accumulation rate; corresponding nonphosphorus peaks are less discernible at 2-3 Ma. Therefore as seen from the viewpoint of the deep-sea Pacific, the latest Miocene southern hemisphere ice buildup had a far more profound effect upon chemical delivery to the deep Pacific than did the plio-Pleistocene buildup of northern hemisphere ice, which appears mainly to have increased terrigenous accumulation rates for sites nearer to continental margins or in smaller oceans.

Interestingly, the P peak at 5-6 Ma also corresponds to deepening of the Pacific Ocean CCD [Heath et al., 1977], expansion of the Antarctic ice sheet at ~6 Ma [Mayewski, 1975], desiccation of the Mediterranean [Ryan et al., 1974], cessation of deposition of the Monterey Formation (California) and related circum-Pacific organic-rich deposition [Barron et al., 1986], and increase in organic carbon accumulation rate at 6 Ma [Heath et al., 1977; Arthur and Jenkyns, 1981]. These events are clearly related. Ice sheet buildup and consequent intensification of circulation coupled with lowered sea level would increase dissolved calcite supply to the deep sea [Worsley and Davies, 1979], close the then constricted Strait of Gibraltar, and shoal, aerate, and destroy oxygen-minimum zone type [Piper and Codispoti, 1975] organic accumulation in the Monterey and related basins, thereby increasing dissolved P supply to the deep sea. A rise in sea level at 4-5 Ma terminated the deep-sea

TABLE 5. Calculation of the Total Amount of Riverine Phosphorus to Reach the Pacific Deep Sea

	World Ocean Total	Equatorial Pacific* 7°N-4°S	North Pacific*
area	3.62×10^8 km^2	0.17×10^8 km^2	0.49×10^8 km^2
% of world ocean area		4.7	13.6
total global riverine P influx, Lerman et al. [1975] and Meybeck [1982]	1.8×10^{15} g/ka† 9.0×10^{15} g/ka‡	85 µg/cm^2/ka 423 µg/cm^2/ka	245 µg/cm^2/ka 1224 µg/cm^2/ka
P flux (10 Ma average, this study)		1039 µg/cm^2/ka	286 µg/cm^2/ka
total P influx		1.76×10^{14} g/ka	1.4×10^{14} g/ka
% total global riverine P influx, Lerman et al. [1975] and Meybeck [1982]		9.8 2.0	7.8 1.6

*[Berger and Winterer, 1974, Figure 1].
†Dissolved P plus particulate P.
‡Dissolved P plus total organic particulate P.

Pacific P peak and reflooded the Mediterranean but did not cause appreciable shoaling of the CCD or reinstitute Pacific-rim Monterey-type organic deposition; perhaps much of the Antarctic ice volume increase was essentially permanent and the sea level rise was not great. However, deposition of P rich sediments did again increase on the reflooded shelves of the Atlantic margin [Riggs, 1984].

No simple paleoceanographic scenario based on convergent lines of evidence can be constructed to explain the P accumulation rate peak at 2-3 Ma. However, it too corresponds to a sharp regression of the seas, marking the beginning of the rapid oscillatory growth and decay of northern hemisphere ice sheets that continues to the present [Mayer et al., 1986; Haq et al., 1987]. This regression would also have increased P supply to the deep sea.

Where is the Phosphorus?

The results of this study support the contention of Moody et al. [1981] that the majority of the P content of biogenic-rich, terrigenous-poor pelagic sediments of the Pacific Ocean (and by implication, the other oceans) is derived from syn-depositionally and postdepositionally destroyed organic matter. The transient organic matter serves as a P transport conduit from surface ocean to seafloor, liberating dissolved P in the bioturbated layer as the organic matter is destroyed for renucleation onto other sites in the P-saturated lower levels of the bioturbated layer. The contention [Moody et al., 1981; Froelich, 1982] that planktonic foraminifera do not incorporate significant quantities of P into their mineral structure has been confirmed by others. Palmer et al. [1985] and Sherwood et al. [1987] have demonstrated, using the ion microprobe, that planktonic foraminiferal calcite contains only ~10 ppm P.

Given that foraminiferal, radiolarian, and diatom skeletons contain no significant P, i.e., <50 ppm, and hence cannot be a major contributor to deep-sea sediment P flux, only coccoliths remain as a potential P transport agent to augment organic matter P transport. Coccolith skeletons appear to have ~400 ppm P associated with them [Froelich, 1982]. Unfortunately, coccoliths have not been directly measured

for their P content using the ion microprobe nor do any of our data directly support a very low P content for coccolith calcite, so that our suggestion that coccoliths contain no significant P incorporated into their crystal structure is more indirect and subtle; indeed, coccolith-enriched sediments do seem to contain a higher P content (Table 2). Froelich [1982] assigned a P content of ~400 ppm to coccoliths compared to ~50 ppm for foraminifera based on laboratory size fractionation of foraminifera and coccoliths. However, the high P content of the coccoliths is either associated with the organic membrane [Honjo, 1977] known to encapsulate coccoliths or to the very low permeability imparted to coccolith-rich sediments due to the small size and platy shape of the coccoliths that favor nucleation rather than escape of organically derived P from the bioturbated layer. Our results extend Froelich's findings to the natural bottom sediment sorting processes of the Pacific Ocean. Table 2 shows that for all biogenic-containing sites for which they were measured, samples containing the highest ratio of coarse (>5 μ) to fine (<5 μ) sediment in the terrigenous fraction are or are close to those with the lowest P content. We interpret this as evidence of winnowing of fines that leads to enhanced permeability and hence enhanced organic P loss. The Initial Report volumes [Winterer et al., 1971; Hays et al., 1972; Larson et al., 1975; Thiede et al., 1981; Barron et al., 1986; Pisias and Prell, 1986] confirm that these low-P intervals contain "porous foraminiferal-enriched/matrix-depleted sands."

To our knowledge, opaline skeletons of diatoms and radiolarians have not been analyzed for their P content with the ion microprobe. Our results (Table 2) demonstrate that samples most enriched in opal contain the lowest ratios of P to noncarbonate sediment except for the two equatorial sites below the CCD (65 and 66) both of which are clearly P enriched by the process of destruction of organic matter and nucleation of P discussed above. We can therefore conclude that biogenic opal most probably contains no significant P, i.e., <50 ppm.

An especially graphic example of opal enrichment/winnowing is sample H10 of shallow water site 586. This sample contains the lowest P content of any sample measured for this study. H10 also shows both strong evidence of winnowing (no terrigenous fines) and is the most opal-enriched sample at that site (presumably robust radiolarians rather than the more fragile diatoms because of the winnowing). We would interpret this sample as a permeable foraminiferal/radiolarian "lag deposit" from which the P containing "fines" (organic matter, coccoliths, windblown dust) were either bypassed from or destroyed within the bioturbated layer via scavenge and scour in the well-aerated bottom sediment.

CONCLUSION

The P content of deep-sea sediments is proportional to organic and mineral particle delivery to the seafloor and to the amount of coccolith carbonate dissolved from the seafloor. It is inversely proportional to the grain size of the skeletal and mineral particles delivered. Therefore the actual P content of a particular sediment at a given site depends upon our understanding how the total of oceanographic variables at that site have interacted.

Future planned work involves examining the potential linkages between phosphorus availability, tectonics, and glaciation as suggested by Worsley et al. [1986]. The results presented in this paper will be used along with data and conclusions of other investigators toward a coherent explanation for the coupling among phosphorus availability, tectonics, and glaciation.

Acknowledgments. Samples and Gamma Ray Attenuation Porosity Evaluator (GRAPE) data (porosity and bulk density) were provided by Deep Sea Drilling Project (Scripps Institute of Oceanography), and Woods Hole Oceanographic Institute. Phosphorus measurements were completed in Battelle Columbus Division through the help and cooperation of Jeffrey Means and Greg Headington. Battelle Memorial Institute is thanked for their generous support of manuscript preparation.

REFERENCES

Arthur, M. A., and H. C. Jenkyns, Phosphorites and paleoceanography, Proceedings of 26th International Geological Congress, Geology of Oceans Symposium, Oceanol. Acta, 4, 83-96, 1981.

Barron, J. A., G. Keller, and D. A. Dunn,

A multiple microfossil biochronology for the Miocene, The Miocene Ocean: Paleoceanography and Biogeography, Mem. Geol. Soc. Am., 163, 21-36, 1985.

Barron, J., C. A. Nigrini, A. Pujos, T. Saito, F. Theyer, E. Thomas, Synthesis of biostratigraphy, central equatorial Pacific, Deep Sea Drilling Project Leg 85: Refinement of Oligocene to Quaternary biochronology, Initial Rep. Deep Sea Drill. Proj., 85, 905-934, 1986.

Bender, M. L., and D. W. Graham, Long-term constraints on the global marine carbonate system, J. Mar. Res., 36, 551-567, 1978.

Bender, M. L., and L. D. Keigwin, Speculations about the upper Miocene change in abyssal Pacific dissolved biocarbonate $\delta^{13}C$, Earth Planet. Sci. Lett., 45, 383-393, 1979.

Berger, W. H., Deep-sea carbonates: Dissolution facies and age constancy, Nature, 236, 392-395, 1972.

Berger, W. H., and E. L. Winterer, Plate stratigraphy and the fluctuating carbonate line, Spec. Publ. Int. Assoc. Sedimentol., 1, 11-48, 1974.

Berggren, W. A., and J. van Couvering, A Cenozoic time scale: Some implications for geology and paleobiography, Lethaia, 5, 195-215, 1972.

Bernas, B., A new method for decomposition and comprehensive analysis of silicates by atomic absorption spectrometry, Annal. Chem., 40, 1532-1686, 1968.

Brewster, N. A., Cenozoic biogenic silica sedimentation in the Antarctic Ocean based on two deep sea drilling project sites, M.S. thesis, 99 pp., Oreg. State Univ., Corvallis, 1977.

Brewster, N. A., Cenozoic biogenic silica sedimentation in the Antarctic Ocean, Geol. Soc. Am. Bull., 91, 337-347, 1980.

Broecker, W. S., and T. H. Peng, Tracers in the Sea, 690 pp., Eldigio, New York, 1982.

Bronnimann, P., and J. Resig, A Neogene globigerinacean biochronologic time-scale of the southwestern Pacific, Initial Rep. Deep Sea Drill. Proj., 7, 1235-1470, 1971.

Bukry, D., Coccolith and silicoflagellates stratigraphy northwestern Pacific ocean, Deep Sea Drilling Project Leg 32, Initial Rep. Deep Sea Drill. Proj., 32, 677-702, 1975.

Burnett, W. C., Phosphorite deposits from the sea floor off Peru and Chile: Radiochemical and geochemical investigations concerning their origin, Ph.D. thesis, 164 pp., Univ. of Hawaii, Honolulu, 1974.

Burnett, W. C., Geochemistry and origin of phosphorite deposits from off Peru and Chile, Geol. Soc. Am. Bull., 88, 813-823, 1977.

Cepek, P., Mesozoic calcareous-nannoplankton stratigraphy of the central north Pacific (mid-Pacific mountains and Hess rise), Deep Sea Drilling Project Leg 62, Initial Rep. Deep Sea Drill. Proj., 32, 397-418, 1981.

Chaboudy, L. R., Long-term phosphorus flux to Neogene Antarctic and Pacific deep sea sediments, M.S. thesis, 112 pp., Ohio Univ., Athens, 1984.

Ciesielski, P. F., Biostratigraphy and paleoecology of Neogene and Oligocene silicoflagellates from cores recovered during Antarctic Leg 28, Deep Sea Drilling Project, Initial Rep. Deep Sea Drill. Proj., 28, 625-692, 1975.

Corliss, B. H., and C. D. Hollister, A paleoenvironmental model for Cenozoic sedimentation in the central north Pacific, in The Ocean Floor, edited by R. A. Scrutton and M. Talwani, pp. 277-304, John Wiley, New York, 1982.

Davies, T. A., and T. R. Worsley, Paleoenvironmental implications of oceanic carbonate sedimentation rates, Spec. Publ. Soc. Econ. Paleontol. Mineral., 32, 169-179, 1981.

De Lange, G. J., Early diagenetic reactions in interbedded pelagic and turbiditic sediments in the Nares Abyssal Plain (western north Atlantic): consequences for the composition of sediment and interstitial water, Geochem. Cosmochim. Acta, 50, 2543-2561, 1986.

Doyle, P. S., G. G. Kennedy, and W. R. Riedel, Stratigraphy, Initial Rep. Deep Sea Drill. Proj., 26, 825-905, 1979.

Dunsworth, M. J., P. S. Doyle, and W. R. Riedel, Ichthyoliths from some NW Pacific sediments, Leg 32, Initial Rep. Deep Sea Drill. Proj., 32, 853-863, 1975.

Froelich, P. N., M. L. Bender, N. A. Luedtke, G. R. Heath, and T. DeVries, Marine phosphorus cycle, Am. J. Sci., 282, 474-511, 1982.

Gordon, A. L., Recent physical oceano-

graphic studies of Antarctic water, in Antarctic Research of American Association for the Advancement of Science, edited by L. Quam, pp. 609-629, Washington D. C., 1971a.

Gordon, A. L., Oceanography of Antarctic Waters, Antarct. Oceanogr., 15, 169-203, 1971b.

Gulbrandsen, R. A., C. E. Roberson, and S. T. Neil, Time and crystallization of apatite in seawater, Geochim. Cosmochim. Acta, 48, 213-218, 1984.

Haq, B. U., Jurassic to recent nannofossil biochronology, in Nannofossil Biostratigraphy, Benchmark Papers in Geology, Vol. 78, edited by B. U. Haq, pp. 358-378, Hutchinson Ross, Stroudsburg, Pa., 1983.

Haq, B. U., J. Hardenbol, and P. R. Vail, Chronology of fluctuating sea levels since the Triassic (250 million years ago to present), Science, 235, 1156-1167, 1987.

Hays, J. D., and Shipboard Scientific Party, Initial Rep. Deep Sea Drill. Proj., 7, 1757 pp., 1972.

Heath, G. R., Dissolved silica and deep-sea sediments, Studies in Paleoceanography, Spec. Publ. Soc. Econ. Paleontol. Mineral., 20, 77-93, 1974.

Heath, G. R., T. C. Moore, and T. H. van Andel, Carbonate accumulation and dissolution in the equatorial Pacific during the past 45 million years, in The Fate of Fossil Fuel CO_2 in the Oceans, edited by N. R. Anderson and A. Malahoff, pp. 627-640, Plenum, New York, 1977.

Holland, H. D., The Chemistry of the Atmosphere and Oceans, 351 pp., John Wiley, New York, 1978.

Honjo, S., Biogenic carbonate particles in the ocean; do they dissolve in the water column, in The Fate of Fossil Fuel CO_2 in the Oceans, edited by N. R. Anderson and A. Malahoff, pp. 269-294, Plenum, New York, 1977.

Jackson, M. L., Soil Chemical Analysis - Advanced Course, 2nd ed., pp. 110-125, M. Jackson, Madison, Wis., 1979.

Jahnke, R. A., The synthesis and solubility of carbonate fluorapatite, Am. J. Sci., 284, 58-78, 1984.

Jahnke, R. A., S. R. Emerson, K. K. Roe, and W. C. Burnett, The present day formation of apatite in Mexican continental margin sediments, Geochim. Cosmochim. Acta, 47, 259-266, 1983.

Jenkins, D. G., and W. N. Orr, Planktonic foraminiferal biostratigraphy of the eastern equatorial Pacific, Leg 9, Initial Rep. Deep Sea Drill. Proj., 9, 1059-1196, 1972.

Kemp, E. M., and P. J. Barrnett, Antarctic glaciation and early Tertiary vegetation, Nature, 258, 507, 1975.

Kennett, J. P. (Ed.), The Miocene Ocean: Paleoceanography and biogeography, Mem. Geol. Soc. Am., 163, 337 pp., 1985.

Kennett, J. P., N. J. Shackleton, S. V. Margolis, D. E. Goodney, W. C. Dudley, and P. M. Kroopnick, Late Cenozoic oxygen and carbon isotopic history and volcanic ash stratigraphy: DSDP Site 284, south Pacific, Am. J. Sci., 279, 52-69, 1979.

Krom, M. D., and R. A. Berner, The diagenesis of phosphorus in a nearshore marine sediment, Geochim. Cosmochim. Acta, 45, 207-216, 1981.

Larson, R. L., R. Moberly, and Shipboard Scientific Party, Initial Reports of the Deep Sea Drilling Project, Vol. 32, edited by R. L. Larson, R. Moberly et al., 980 pp., U.S. Government Printing Office, Washington, D. C., 1975.

Leinen, M., Biogenic silica sedimentation in the central equatorial Pacific during the Cenozoic, M.S. thesis, 136 pp., Oreg. State Univ., Corvallis, 1975.

Leinen, M., and D. Stakes, Metal accumulation rates in the central equatorial Pacific during Cenozoic times, Geol. Soc. Am. Bull., 90, 357-375, 1979.

Lerman, A., F. T. MacKenzie, R. M. Garrels, Modeling of geochemical cycles: Phosphorus as an example, Quantative Studies in Geological Science, Mem. Geol. Soc. Am., 142, 205-218, 1975.

Mach, D. L., A. Ramirez, and H. D. Holland, Organic phosphorus and carbon in marine sediments, Am. J. Sci., 278, 429-441, 1987.

Mayer, L. A., T. H. Shipley, and L. Winterer, Equatorial Pacific seismic reflectors as indicators of global oceanographic events, Science, 233, 761-764, 1986.

Mayewski, P. A., Glacial geology and late Cenozoic history of the Transantarctic Mountains, Ohio State Univ. Inst. Polar Stud., Antarct. Rep. 56, 105 pp., Ohio State Univ., Columbus, 1975.

Menard, H. W., Marine Geology of the

Pacific, 271 pp., McGraw-Hill, New York, 1964.
Meybeck, M., Carbon, nitrogen, and phosphorus transport by world rivers, Am. J. Sci., 282, 401-450, 1982.
Moody, J. B., T. R. Worsley, and P. R. Manoogian, Long-term phosphorus flux to deep sea sediments, J. Sediment. Petrol., 51, 307-312, 1981.
Muller, C., Miocene to Pleistocene silicoflagellates from the central north Pacific, Deep Sea Drilling Project Leg 62, Initial Rep. Deep Sea Drill. Proj., 62, 361-364, 1981.
Palmer, M. R, Rare earth elements in foraminifera tests, Earth Planet. Sci. Lett., 73, 285-298, 1985.
Piper, D. Z., and L. A. Codispoti, Marine phosphorite deposits and the nitrogen cycle, Science, 188, 15-18, 1975.
Pisias, N. G., and W. L. Prell, Changes in calcium carbonate accumulation in the equatorial Pacific during the late Cenozoic: Evidence from HPC Site 572, in The Carbon Cycle and Atmospheric CO_2: Natural Variations Archean to Present, Geophys. Monogr., Vol. 32, edited by E. T. Sundquist and W. S. Broecker, pp. 443-454, AGU, Washington, D. C., 1985.
Pisias, N. G., and W. L. Prell, High resolution carbonate records from the hydraulic piston cored section of site 572, Initial Rep. Deep Sea Drill. Proj., 85, 711-722, 1986.
Prince, R. A., G. R. Heath, and M. Kominz, Paleomagnetic studies of central north Pacific sediment cores: Stratigraphy, sedimentation rates, and origin of magnetic instabilities, Geol. Soc. Am. Bull., 91, 1789-1835, 1980.
Ramsey, C. A., P. S. Doyle, and W. R. Riedel, Ichtholiths in late Mesozoic pelagic sediments, mainly from Italy, Micropaleontology, 22, 129-142, 1976.
Riedel, W. R., and A. Sanfilippo, Cenozoic radiolaria from the western tropical Pacific, leg 7, Initial Rep. Deep Sea Drill. Proj., 7, 1529-1672, 1971.
Riggs, S. R., Paleoceanographic model of Neogene phosphorite deposition, U.S. Atlantic continental margin, Science, 223, 123-131, 1984.
Ryan, W.B.F., et al., A paleomagnetic assignment of Neogene stage boundaries and the development of isochronous datum planes between the Mediterranean, the Pacific and Indian Oceans in order to investigate the response of the world ocean to the Mediterranean "salinity crisis," Riv. Ital. Paleontol., 80, 631-688, 1974.
Sandstrom, M. W., Diagenesis of organic phosphorus in marine sediments: Implications for the global carbon and phosphorus cycles, in Cycling Carbon, Nitrogen, Sulfur, Phosphorus, edited by J. R. Freney and I. E. Galbally, pp. 133-141, Springer-Verlag, New York, 1982.
Shafkin, S., Nannofossil biostratigraphy of the southwest Pacific, Deep Sea Drilling Project leg 30, in Initial Rep. Deep Sea Drill. Proj., 30, 549-598, 1975.
Shapiro, L., Rapid analysis of silicate, carbonate and phosphate rocks (revised), U.S. Geol. Surv. Bull., 1401, 76 pp., 1975.
Sherwood, B. A., S. L. Sager, and H. D. Holland, Phosphorus in foraminiferal sediments from north Atlantic ridge cores, Geochim. Cosmochim. Acta, 51, 1861-1866, 1987.
Smith, S. V., Phosphorus versus nitrogen limitation in the marine environment, Limnol. Oceanogr., 29, 1149-1160, 1984.
Taylor, S. R., Abundance of chemical elements in the continental crust: A new table, Geochim. Cosmochim. Acta, 28, 1273-1285, 1964.
Thiede, J., T. L. Vallier, and Shipboard Scientific Party, Initial Reports of the Deep Sea Drilling Project, Vol. 62, edited by J. Thiede and T. L. Vallier, 856 pp., U.S. Government Printing Office, Washington, D. C., 1981.
van Andel, T. H., G. R. Heath, T. C. Moore, Cenozoic history and paleoceanography of the central equatorial Pacific ocean, Mem. Geol. Soc. Am., 143, 134 pp., 1975.
Vincent, E., J. S. Killingley, and W. H. Berger, The magnetic epoch-6 carbon shift: A change in the oceans $^{13}C/^{12}C$ ratio 6.2 million years ago, Mar. Micropaleontol., 5, 185-203, 1980.
Winterer, E. L., and Shipboard Scientific Party, Initial Reports of the Deep Sea Drilling Project, Vol. 7, edited by E. L. Winterer et al., 1757 pp., U.S. Government Printing Office, Washington, D. C., 1971.
Worsley, T. R., and T. A. Davies, Cenozoic sedimentation in the Pacific ocean: Steps toward a quantitative evaluation,

J. Sediment. Petrol., 49, 1131-1146, 1979.

Worsley, T. R., R. D. Nance, and J. B. Moody, Tectonic cycles and the history of the Earth's biogeochemical and paleoceanographic record, Paleoceanography, 1, 233-263, 1986.

L. R. Chaboudy, Jr., Amoco Production Company, P.O. Box 3092, Houston, TX 77253.

J. B. Moody, Battelle Memorial Institute, 505 King Avenue, Columbus, OH 43201.

T. R. Worsley, Department of Geological Sciences, Ohio University, Athens, OH 45701.

(Received January 16, 1987; revised December 7, 1987; accepted December 18, 1987.)